ISSN 0031-918X, Physics of Metals and Metallography, 2022, Vol. 123, No. 1, pp. 50–56. © Pleiades Publishing, Ltd., 2022.
Russian Text © The Author(s), 2022, published in Fizika Metallov i Metallovedenie, 2022, Vol. 123, No. 1, pp. 55–62.

STRUCTURE, PHASE TRANSFORMATIONS, AND DIFFUSION

Effect of the Temperature of Mechanical Tests on the Properties of the Nanocrystalline Cu–14Al–3Ni Alloy Subjected to High Pressure Torsion

A. E. Svirid[a, *], V. G. Pushin[a, b], N. N. Kuranova[a, b], N. V. Nikolaeva[a], and A. N. Uksusnikov[a]

[a] *Mikheev Institute of Metal Physics, Ural Branch, Russian Academy of Sciences, Ekaterinburg, 620108 Russia*

[b] *Ural Federal University Named after the First President of Russia B.N. Yeltsin, Ekaterinburg, Russia*

**e-mail: svirid2491@rambler.ru*

Received July 13, 2021; revised August 26, 2021; accepted September 3, 2021

Abstract—The tensile tests in combination with the electron microscopy and X-ray technique have provided data on the mechanical properties of the ultrafine-grained (UFG) shape-memory Cu–14 wt % Al–3 wt % Ni alloy at different temperatures and its fracture character. The UFG structure in the alloy has formed during severe plastic deformation performed by high pressure torsion. The study has shown two variants of the mechanical behavior of the UFG alloy depending on the temperature and strain rate during mechanical testing. The first case is the deformation of the alloy in the martensitic state at moderate test temperatures (300, 423, 473 K). This stage is characterized by a high hardening coefficient and moderate uniform relative elongation and reduction. The second case is deformation at higher test temperatures (573, 673 K). It is characterized mainly by large uniform localized plastic deformation and moderate hardening due to dynamic recrystallization.

Keywords: copper alloys, thermoelastic martensitic transformation, high pressure torsion, shape memory effect, structure, temperature dependence of mechanical properties

DOI: 10.1134/S0031918X22010136

INTRODUCTION

Temperature, mechanical, and other external conditions that provide thermoelastic martensitic transformations (TMTs) allow for a number of unusual physical phenomena of practical importance in various alloys. The cyclically reversible TMT-induced shape memory effect (SME), giant superelasticity, damping, and caloric effects (including magnetocaloric, electrocaloric, barocaloric, and elastocaloric) mark these smart alloys off as a special separate class of innovatively attractive structural polyfunctional metal materials that are in demand for efficient high-tech and environmentally friendly technologies [1–10].

Modern technology needs to develop smart alloys that can be used in products, devices, and mechanisms in wide appropriate heat and pressure ranges and under other service conditions. However, a critical disadvantage of most polycrystalline smart materials (except for binary titanium nickelide alloys) is their low plasticity and brittleness, which do not allow for their unique effects to be implemented in either cyclic multiple or even single applications. Therefore, developing production techniques, selecting optimal alloying, and heat-mechanical treatments of various polycrystalline smart materials for their plastification are getting more and more important for their subsequent various commercial applications.

These economically promising materials are the copper shape-memory β alloys of Cu–Al–Ni, Cu–Zn–Al, and other systems, where TMT occur and which have much lower cost, better thermal and electrical conductivity, and processability as compared to titanium nickelide alloys [2, 3, 11]. The single-crystal copper β alloys exhibit excellent SME characteristics. However, these polycrystalline alloys exhibit low ductility, fracture resistance, and fatigue life in their normal coarse-grained state [3, 11]. One of the key factors that limit the practical application of shape memory alloys is their intercrystalline brittleness [3].

The formation of an ultrafine-grained (UFG) structure is known to noticeably improve the strength and plastic characteristics of the shape memory alloys based on titanium nickelide [12]. Advanced heat-deformation techniques are used to form a UFG structure in these alloys. These techniques are based on a number of severe plastic deformation techniques, including pressing or high-pressure torsion (HPT) and, in practice, multipass rolling, and drawing to form strips, rods, and wires.

Our recent studies [12–17] have also shown a significant embrittlement attenuation in copper shape memory alloys, which was achieved by a considerable reduction in grain size and an increase in the grain boundary length during severe plastic deformation. Various other techniques, including alloying with additives, heat treatments, rapid quenching, powder metallurgy, and others, were unsuccessful and did not refine the grain structure of these alloys or improve their ductility significantly [18–27]. The mechanical behavior of copper shape-memory alloys has not been studied in a wide temperature range. Therefore, this study aims to investigate the effect of the mechanical test temperature on the phase composition, structure, and mechanical properties of the UFG Cu–Al–Ni shape-memory alloy.

EXPERIMENTAL

The alloy of nominal chemical composition Cu–14 wt % Al–3 wt % Ni, which was in the austenitic state at room temperature (RT), was melted from high-purity components, such as Cu, Al, and Ni (99.99% purity). Spectroscopy showed that it contained 13.95% Al, 3.02% Ni, and Cu for balance (wt %). The alloy ingot was subjected to hot forging at 1173–1273 K to form a 20 × 20-mm-section bar, which was quenched in water from 1223 K for 10 min. The grain structure refinement in the alloy was achieved by the RT HPT at 6 GPa after 10 revolutions. The deformation was performed in flat anvils with a "hole" (cylindrical dimple in the bottom anvil) made of metal–ceramic of the VK-6 type (92 HRC). Samples for HPT were fabricated in the shape of disks 20 mm in diameter and 1.2 mm thick. Their thicknesses were reduced to 0.5 mm after 10 revolutions. The true strain at the half radius was 6 units. Flat specimens 10 mm long, 0.25 mm thick, and 1 mm wide for tensile tests were cut at a half radius of the original disc using an electrospark machine. Their gage length was 4.5 mm. The sample surface before testing was polished with diamond paste. The testing velocity V_{test} was 10^{-3} and 10^{-4} s^{-1}. The critical temperatures of the beginning (M_s, A_s) and end (M_f, A_f) of the forward (M_s, M_f) and reverse (A_s, A_f) TMTs were determined by cyclic temperature measurements of the magnetic susceptibility (in the cooling–heating–cooling cycles) $\chi(T)$ and electrical resistivity $\rho(T)$ at a rate close to 5 K/min (Table 1). The structure and phase composition were studied by X-ray diffraction (XRD), optical metallography (OM), transmission electron microscopy (TEM), and scanning electron microscopy (SEM). The XRD was carried out in monochromatic copper $K\alpha$ radiation. The TEM was conducted using a Tecnai G^2 30 at an accelerating voltage of 300 kV. The SEM was performed at an accelerating voltage of 30 kV using a Quanta 200 microscope equipped with the Pegasus system. Vickers microhardness (HV) measurements were performed on a Micromet 5101 tester equipped with a pyramidal diamond indenter, at a load of 1 N.

Table 1. Critical temperatures of the onset (M_s, A_s) and the end (M_f, A_f) of TMTs in the Cu–14Al–3Ni alloy after various treatments

Treatment	M_s, K	M_f, K	A_s, K	A_f, K	ΔT*, K
Quench. 1223 K	250	230	265	285	35
HPT, 10 revs.	320	300	400	440	110

* $\Delta T = 1/2\{(A_s + A_f) - (M_s + M_f)\}$.

RESULTS AND DISCUSSION

The cast and forged copper β alloy undergoes the $\beta \rightarrow \beta_1 + \gamma_2$ decomposition (at temperatures above T_{ED} close to 840 K) and the $\beta_1 \rightarrow \alpha + \gamma_2$ eutectoid decomposition (ED; at temperatures below T_{ED}) (Fig. 1a) during subsequent air cooling of the ingot or forging, which agrees with the known data [2].

However, quenching of the alloy after hot forging can prevent eutectoid decomposition (Fig. 1b). The β austenite is known to undergo two consecutive "disorder–order" phase transitions ($\beta \rightarrow \beta_2(B2) \rightarrow \beta_1(D0_3)$) even during quenching upon rapid cooling at temperatures above T_{ED} and M_s [3]. The multinucleation transition mechanism results in the formation of

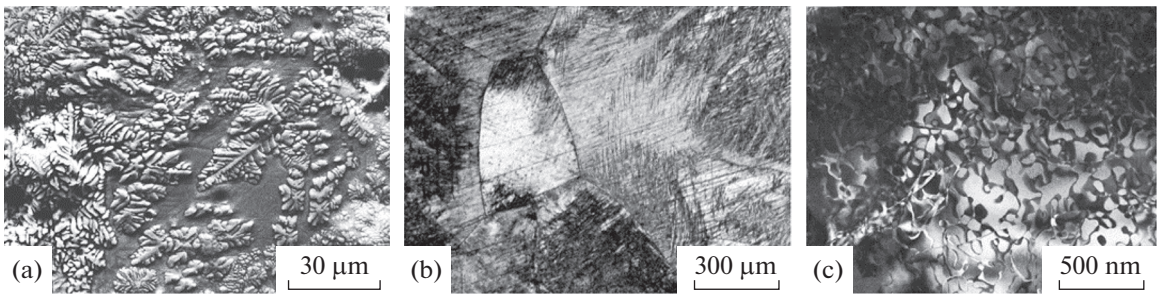

Fig. 1. (a) SEM image taken in backscattered electrons, (b) OM image, and (c) TEM image of the Cu–14Al–3Ni alloy structure in the (a) cast and (b), (c) quenched austenitic states.

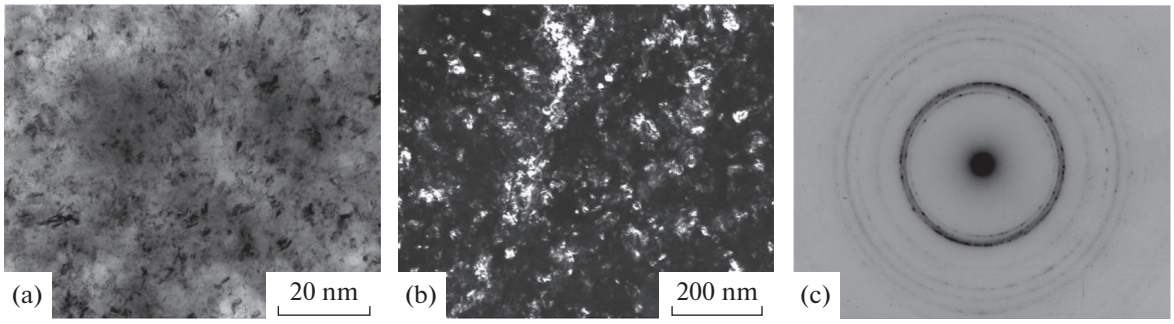

Fig. 2. (a) Bright-field and (b) dark-field TEM images of the microstructure and (c) corresponding electron diffraction (SAED) pattern of the Cu–14Al–3Ni alloy after quenching from 1223 K and HPT to 10 revolutions.

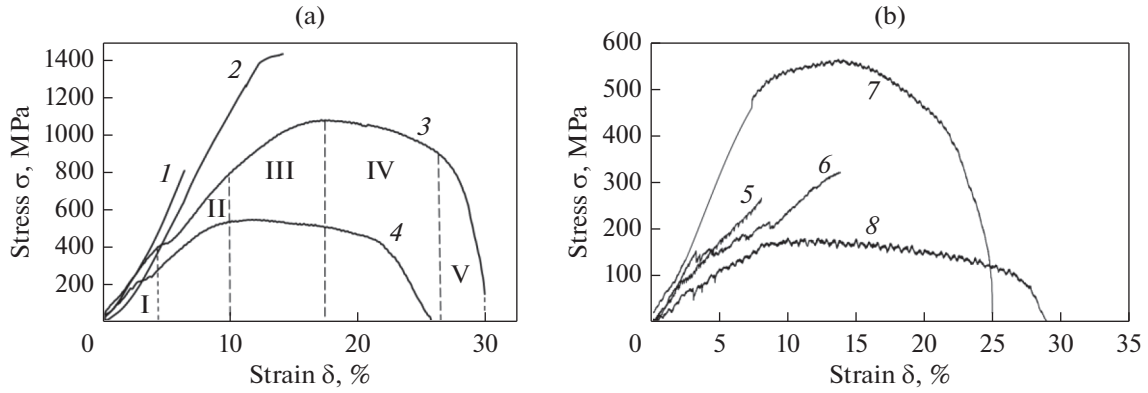

Fig. 3. Relative stress–strain curves of the Cu–14Al–3Ni alloy after HPT to 10 revolutions, at (a) $V_{test} \sim 1 \times 10^{-3}$ s^{-1} and temperatures of (*1*) 300, (*2*) 423, (*3*) 573, (*4*) 673 K; and at (b) $V_{test} \sim 10^{-4}$ s^{-1} and (*5*) 423, (*6*) 473, (*7*) 573, and (*8*) 673 K. I–V are the stages of deformation.

the special substructure of antiphase domains visualized by the appearance of their boundaries (APBs) on the dark-field TEM images taken in superstructure reflections (Fig. 1c). The long-range atomic order of the ordered austenitic phase is inherited by the martensite during TMT, which provides the effects of orientational crystal–structural reversibility and phase thermoelasticity in alloys [1–6].

XRD analysis indicates two martensitic phases in the quenched β_1 alloy at temperatures below M_s close to 250 K (Table 1): β_1' (18*R*) (long-period monoclinic lattice parameters that are close to $a = 0.4450$ nm, $b = 0.5227$ nm, $c = 3.8050$ nm, $\beta = 91.0°$) and γ_1' (2*H*) (orthorhombic lattice parameters that are close to $a = 0.4390$ nm, $b = 0.5190$ nm, $c = 0.4330$ nm). The HPT to 10 revolutions at RT was found to cause deformation TMT resulting in a mixture of three martensitic α', β_1', and γ_1' phases. The Bragg reflections detected are significantly broadened (a halfwidth up to 2 degrees) and they coincide with the strongest lines of these martensitic phases.

TEM studies showed that 10-revolution HPT resulted in the formation of a uniform nanograined martensitic structure in the Cu–14Al–3Ni alloy. This structure is characterized by a circular distribution of reflections in the electron diffraction patterns (see Fig. 2). Quantitative analysis of bright and dark-field TEM images of the alloy microstructure after HPT to 10 revolutions shows that the sizes of the randomly oriented nanograins vary from 10 to 80 nm. Their average size is about 30 nm. The larger of them contain lamellar nanotwins. Indexing of electron diffraction patterns also showed mainly β_1' and γ_1' martensitic phases in the nanocrystalline structure of the alloy. The ring distribution of reflections indicates the presence of nanophases forming a misoriented ultrafine-grained structure.

The HPT-deformed alloy was tested at two tensile rates $V_{test} \sim 10^{-3}$ (Fig. 3a) and 10^{-4} s^{-1} (Fig. 3b) in a wide temperature range 300–673 K below T_{ED} (Fig. 3, Table 2). The mechanical behavior of the UFG alloy in the martensitic state (at (*1*) 300 K, (*2*), (*5*) 423 K, (*6*) 473 K) and austenitic state (at (*3*), (*7*) 573 K, (*4*),

Table 2. Tensile test results at elevated temperatures for the UFG Cu–14Al–3Ni alloy after HPT to 10 revolutions

No.	T_{test}, K	Rate, s^{-1}	σ_u, MPa	$\sigma_{0.2}$, MPa	$d\sigma/d\varepsilon_M$, MPa	σ_M, MPa	δ_u, %	δ_{c1}, %	δ_{c2}, %	δ, %	ε_M, %
1	300	10^{-3}	800	–	20.0	–	5	–	–	5	–
2	423	10^{-3}	1450	1000	12.8	–	6	–	–	6	–
3	573	10^{-3}	1100	800	5.3	400	8	9	3	20	1.5
4	673	10^{-3}	580	400	3.2	200	6	10	4	20	1.5
5	423	10^{-4}	280	200	4.0	100	6	–	–	6	1.5
6	473	10^{-4}	320	280	2.7	150	11	–	–	11	2.0
7	573	10^{-4}	570	470	1.7	–	6	9	3	18	–
8	673	10^{-4}	170	60	1.6	–	10	15	2	27	–

(*8*) 673 K) was found to differ significantly. The stress–strain ($\sigma-\delta$) curves of the austenitic UFG alloy at elevated temperatures of 573 and 673 K exhibit several typical stages of deformation: (I) elastic, (II; curves *3*, *4*) pseudoelastic with a region or zone of phase flow, (III, up to the ultimate tensile strength σ_u) uniform, and (IV, V) two localized, which exhibit, first, gradual and, then, accelerated softening in the forming wedge-shaped neck region of the tensile specimens. The $\sigma-\delta$ curves of the UFG alloy in the martensitic state at lower test temperatures (300–473 K) differ, first, in hardening $d\sigma/d\varepsilon_M$, which increases with strain and determines the unusual shape of their elastic and pseudoelastic stages (I, II). Then, the III stage of uniform deformation develops starting from the $\sigma_{0.2}$ yield strength. Another obvious difference is that there are no localized deformation stages (IV, V), apparently, due to other mechanisms of plastic deformation and there is no softening effect in the martensitic alloy.

The plateau of the yield of phase observed in the $\sigma-\varepsilon$ diagrams at low V_{test}, which begins with stress σ_M, is known to be due to the shear reorientation of martensitic crystals in the direction of the acting force at temperatures below A_f. At higher temperatures (above A_s, up to M_d, which are the temperatures of deformation martensitic transformation), only the activation of the deformation-induced TMT mechanism is responsible for the appearance of the plateau of the yield of phase.

The deformation of the UFG Cu–14Al–3Ni alloy at RT and 423 K is characterized by a high strain-hardening coefficient and a moderate uniform deformation. The alloy specimens fracture before the process of plastic deformation localization begins. At higher strain temperatures up to 573 and 673 K, on the contrary, the engineering tensile curves take the usual form of tensile curves for steels and alloys (Fig. 3). At higher temperatures, localized strain δ_c increases, and uniform plastic strain δ_u of the UFG Cu–14Al–3Ni alloy decreases (Table 2).

The plateau of the yield of phase observed during the tension of the Cu–14Al–3Ni alloy specimens at 423 and 473 K is not observed at higher deformation temperatures of 573 and 673 K and strain rate of 10^{-4} s^{-1}, because the deformation occurs in stable austenite (above temperatures A_f , M_d; Fig. 3b, curves *7*, *8*) and the deformation is insufficient to induce a TMT (in contrast to curves *5*, *6* in Fig. 3). However, this region appears when V_{test} increases by an order of magnitude, i.e., up to 10^{-3} s^{-1} (curves *3*, *4* in Fig. 3a). In this case, ε_M is 1–2%.

The UFG alloy during tension at 573 K achieves high plasticity when the yield strength $\sigma_{0.2}$ is high enough and the stress at the stage of deformation localization δ_c decreases intensively. This fact seems to be related to the grain boundary slip mechanism in the UFG Cu–14Al–3Ni alloy. However, the alloy did not exhibit superplastic behavior at the chosen temperatures and strain rates. This can be explained by the appreciable dynamic grain growth at elevated test temperatures.

Grain slip, which is a necessary condition for superplasticity, is known to be hindered with increasing grain size. A decrease in V_{test} from 10^{-3} to 10^{-4} s^{-1} decreases the ultimate tensile strength σ_u and yield strength $\sigma_{0.2}$ by more than half, while maintaining the plasticity at the same level (Table 2). We can explain this fact by both the reduced-strain-rate effect and the long time of the elevated-temperature test, which leads to the enlargement of grain sizes.

The microstructure after 673 K static annealing of the HPT-deformed specimens and their tension at 673 K was examined to better understand the structural changes that occur upon testing. The specimen microstructure after its tension was investigated in the region of its uniform deformation and its necking. The average grain size in the UFG alloy after HPT to 10 revolutions and annealing at 673 K (for 30 min) was close to 150 nm (Fig. 4a). The plastic deformation at elevated temperature resulted in significant changes in the grain structure of the alloy microstructure. There

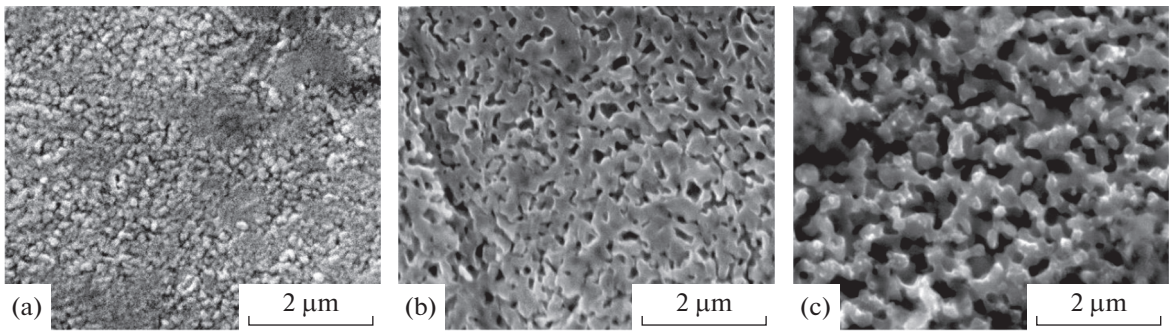

Fig. 4. SEM images of the Cu–14Al–3Ni alloy microstructure after (a) annealing at 673 K for 30 min and (b) tension at 673 K and $V_{test} = 10^{-4}$ s^{-1} in the region of uniform deformation and (c) localized deformation.

were grains of different sizes in the region of uniform deformation, namely, some larger grains of ~450 nm and some smaller grains of about 100 nm, which were newly formed by dynamic recrystallization (Fig. 4b). The boundaries of large grains were curved, and the grains were elongated, as a rule, in one of two directions. Obviously, the boundaries of newly formed grains during dynamic recrystallization begin to migrate, absorbing the initial grains with a high dislocation density. These grains continue to grow and their boundaries continue to migrate under mechanical test conditions at an elevated temperature. Therefore, deformed grains are most likely to be replaced by recrystallized grains in the region of uniform deformation, and this process continues until the specimen fracture. Severe plastic deformation in the neck area caused qualitative changes in the HPT-formed microstructure. The variation in grain sizes, which has previously been observed at the initial stage of dynamic recrystallization, disappeared, and grains acquired better uniform polyhedral faceting (Fig. 4c). The average grain size resulting from dynamic recrystallization when the specimen has been tensioned at 673 K is 250 nm. It is more than 1.5 times higher than the average size determined after 30-min static recrystallization at 673 K.

The *HV* microhardness of the specimens was measured after tensile testing. The hardness was measured on flat grips and in the specimen neck after tensile fracture (Table 3). One can see that *HV* in the specimen neck is higher than that in the grip region after the tension of the Cu–14Al–3Ni alloy at RT; i.e., alloy hardens during its testing. On the contrary, the *HV* values in the neck of the UFG specimens deformed at 673 K are lower than those in the grip region. This fact can be explained by the rapid grain growth caused by dynamic recrystallization in the first case, in contrast to the static annealing without load. The oscillating type of the curves at the stage of plastic flow at elevated temperatures, especially at $V_{test} = 10^{-4}$ s^{-1}, also indirectly indicates the dynamic recrystallization (Fig. 3b).

Fractographic analysis showed ductile fracture with high dispersion of fracture pits (or cups) at elevated deformation temperatures, according to the deformation and microstructural features (Figs. 5b, 5d, 5f, 5h). Fracture at elevated temperatures results in the formation of the fracture surface with small pits (dimples) in all structural states. The fracture surfaces show deep equiaxed elongated pits. The side surface of the specimens after tension exhibits uniformly distributed slip lines in the deformation localization region (Figs. 5a, 5c, 5e, 5g). Therefore, we can conclude that the nature of fracture in the alloys under study depends on the structural state. It is brittle intercrystalline in the martensitic initial coarse-grained state, ductile-brittle in the martensitic UFG state [17], and quasi-brittle (fine-dimple) in the austenitic UFG state at elevated strain temperatures. However, the sizes of dimples (several micrometers) are an order of magnitude larger than the average size of the ultrafine grains of the alloy. This fact indicates a special intercrystalline fracture rather than a transgranular ductile one (which seems to occur along high-angle boundaries in the UFG structure).

Table 3. Microhardness *HV* of the alloy subjected to HPT to 10 revolutions after static annealing (in the grips) and tensile deformation at test temperature (in the neck)

Treatment	T_{test}, K	$\dot{\varepsilon}$, s^{-1}	*HV*, MPa	
			grippers	neck
Quenching from 1223 K	300	10^{-3}	3300	3450
HPT, 10 revs.	300		5650	6550
HPT, 10 revs.	673		4600	3800

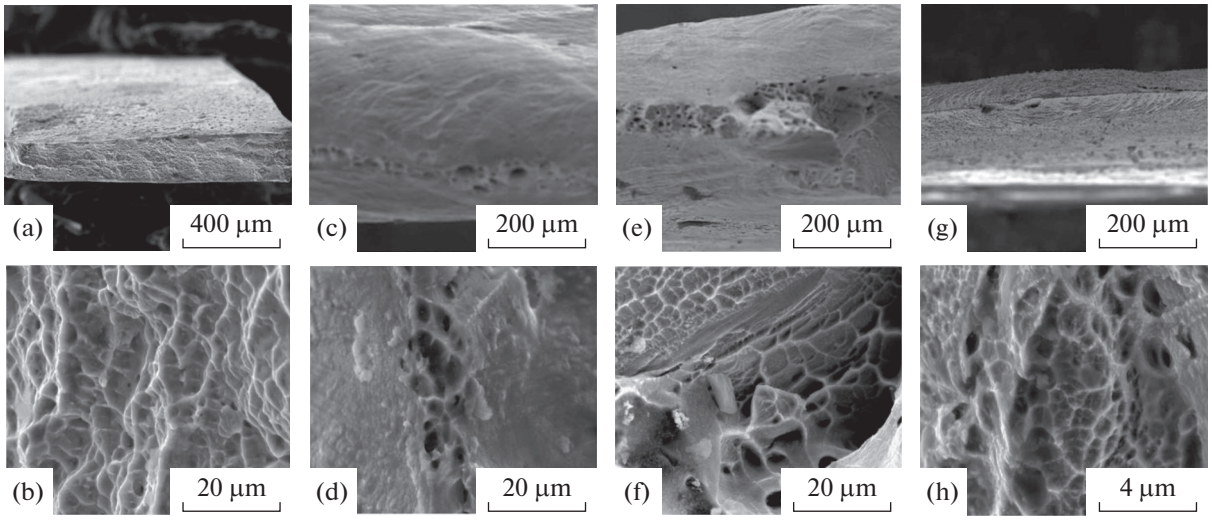

Fig. 5. SEM images (different magnifications) of fracture surfaces of the Cu–14Al–3Ni alloy after tension at $V_{test} = 10^{-4}$ s^{-1} and various temperatures: (a), (b) 423, (c), (d) 473, (e), (f) 573, and (g), (h) 673 K.

CONCLUSIONS

(1) The Cu–14Al–3Ni alloy deformed by HPT to 10 revolutions at a high pressure of 6 GPa was found to exhibit a high strength (σ_u = 800–1400 MPa), high hardening factor, and a moderate uniform relative elongation (up to 10%) during mechanical tensile tests at 300, 423, and 473 K, with its UFG structure to be retained in the martensitic state.

(2) We found the tendency of the UFG austenitic alloy to high-uniform and, especially, localized plastic deformation (18–27%) and moderate hardening (σ_u = 570–580 MPa) due to dynamic recrystallization at elevated test temperatures of 573 and 673 K.

(3) The fractographic studies show that the fracture of the UFG alloy is ductile-brittle (without necking) in the martensitic state and intercrystalline ductile fine-dimpled (with a developed neck) one along the high-angle ultrafine grain boundaries in the austenitic state (at elevated strain temperatures).

ACKNOWLEDGMENTS

The study was performed at the Center of the Collaborative Access "Test Center of Nanotechnologies and Advanced Materials," Institute of Metal Physics, Ural Branch, Russian Academy of Sciences.

FUNDING

This work was performed within the scope of the State Task (theme "Structure," no. AAAA-A18-118020190106-6).

REFERENCES

1. J. Perkins, *Shape Memory Effects in Alloys* (Plenum, London, 1975).
2. Kh. Varlimont and L. Dilei, Martensite Transformations in Alloys Based on Copper, Silver, and Gold (Nauka, Moscow, 1980) [in Russian].
3. K. Ootsuka, K. Simidzu, Yu. Sudzuki, Yu. Sekiguti, Ts. Tadaki, T. Khomma, and S. Miyadzaki, *Shape Memory Alloys* (Metallurgiya, Moscow, 1990) [in Russian].
4. *Engineering Aspects of Shape Memory Alloy*, Ed. by T. W. Duering, K. L. Melton, D. Stockel, and C. M. Wayman, (Butterworth-Heineman, London, 1990).
5. V. N. Khachin, V. G. Pushin, and V. V. Kondrat'ev, *Titanium Nickelide: Structure and Properties* (Nauka, Moscow, 1992).
6. V. G. Pushin, V. V. Kondrat'ev, and V. N. Khachin, *Pre-transitional Phenomena and Martensitic Transformations* (UrO RAN, Yekaterinburg, 1998) [in Russian].
7. E. Bonnot, R. Romero, L. Mañosa, E. Vives, and A. Planes, "Elastocaloric effect associated with the martensitic transition in shape-memory alloys," Phys. Rev. Lett. **100**, 125901 (2008).
8. J. Cui, Y. Wu, J. Muehlbauer, Y. Hwang, R. Radermacher, S. Fackler, M. Wuttig, and I. Takeuchi, "Demonstration of high efficiency elastocaloric cooling with large δT using NiTi wires," Appl. Phys. Lett. **101**, 073904 (2012).
9. L. Mañosa, S. Jarque-Farnos, E. Vives, and A. Planes, "Large temperature span and giant refrigerant capacity in elastocaloric Cu–Zn–Al shape memory alloys," Appl. Phys. Lett. **103**, 211904 (2013).
10. P. Sedlak, H. Seiner, M. Landa, V. Novák, P. Šittner, and L. I. Manosa, "Elastic Constants of bcc Austenite and 2H orthorhombic martensite in CuAlNi shape memory alloy," Acta Mater. **53**, 3643–3661 (2005).
11. R. Dasgupta, "A look into Cu–based shape memory alloys: Present Scenario and future prospects," J. Mater. Res. **29**, No. 16, 1681–1698 (2014).
12. V. Pushin, N. Kuranova, E. Marchenkova, and A. Pushin, "Design and development of Ti–Ni, Ni–Mn–Ga and Cu–Al–Ni-based alloys with high and

low temperature shape memory effects," Materials **12**, 2616–2640 (2019).

13. A. V. Lukyanov, V. G. Pushin, N. N. Kuranova, A. E. Svirid, A. N. Uksusnikov, Yu. M. Ustyugov, and D. V. Gunderov, "Effect of the thermomechanical treatment on structural and phase transformations in Cu–14Al–3Ni shape memory alloy subjected to high-pressure torsion," Phys. Met. Metallogr. **119**, 374–382 (2018).
14. A. E. Svirid, A. V. Luk'yanov, V. G. Pushin, E. S. Belosludtseva, N. N. Kuranova, and A. V. Pushin, "Effect of the temperature of isothermal upsetting on the structure and the properties of the shape memory Cu–14 wt % Al–4 wt % Ni alloy," Phys. Met. Metallogr. **120**, 1159–1165 (2019).
15. A. E. Svirid, V. G. Pushin, N. N. Kuranova, E. S. Belosludtseva, A. V. Pushin, and A. V. Lukyanov, "The effect of plastification of Cu–14Al–4Ni alloy with the shape memory effect in high-temperature isothermal precipitation," Tech. Phys. Lett. **46**, 118–121 (2020).
16. A. E. Svirid, V. G. Pushin, N. N. Kuranova, V. V. Makarov, A. V. Pushin, A. N. Uksusnikov, and A. V. Luk'yanov, "Application of isothermal upset for megaplastic deformation of Cu–Al–Ni β alloys," Tech. Phys. **90**, 1044–1055 (2020).
17. A. E. Svirid, V. G. Pushin, N. N. Kuranova, V. V. Makarov, and A. N. Uksusnikov, "The effect of heat treatment on the structure and mechanical properties of nanocrystalline Cu–14Al–3Ni alloy subjected to high-pressure torsion," Phys. Met. Metallogr. **122**, No. 9, 883–890 (2021).
18. A. Pelosin and A. Riviere, "Structural and mechanical spectroscopy study of the β_1' martensite decomposition in Cu–12% Al–3% Ni (wt %) alloy," J. Alloys Compd. **268**, 166–172 (1998).
19. F. Dagdelen, T. Gokhan, A. Aydogdu, Y. Aydogdu, and O. Adiguzel, "Effect of thermal treatments on transformation behavior in shape memory Cu–Al–Ni alloys," Mater. Lett. **57**, 1079–1085 (2003).
20. Z. Li, Z. Y. Pan, N. Tang, Y. B. Jiang, N. Liu, M. Fang, and F. Zheng, "Cu–Al–Ni–Mn shape memory alloy processed by mechanical alloying and powder metallurgy," Mater. Sci. Eng., A **417**, 225–229 (2006).
21. N. Suresh and U. Ramamurty, "Aging response and its effect on the functional properties of Cu–Al–Ni shape memory alloys," J. Alloys Compd. **449**, 113–118 (2008).
22. R. D. Dar, H. Yan, and Y. Chen, "Grain boundary engineering of Co–Ni–Al, Cu–Zn–Al, and Cu–Al–Ni shape memory alloys by intergranular precipitation of a ductile solid solution phase," Scr. Mater. **115**, 113–117 (2016).
23. P. La Roca, L. Isola, Ph. Vermaut, and J. Malarria, "Relationship between grain size and thermal hysteresis of martensitic transformations in Cu-based shape memory alloys," Scr. Mater. **135**, 5–9 (2017).
24. X. Zhang, X. Zhao, F. Wang, L. Qingsuo, and Q. Wang, "Microstructure, mechanical properties and shape memory effect of Cu–Hf–Al–Ni alloys," Mater. Sci. Technol. **34**, No. 12, 1497–1501 (2018).
25. A. E. Svirid, V. G. Pushin, N. N. Kuranova, A. V. Luk'yanov, A. V. Pushin, A. N. Uksusnikov, and Y. M. Ustyugov, "The structure–phase transformations and mechanical properties of the shape memory effect alloys based on the system Cu–Al–Ni," Mater. Today: Proc. **4**, 4758–4762 (2017).
26. A. E. Svirid, N. N. Kuranova, A. V. Luk'yanov, V. V. Makarov, N. V. Nikolaeva, V. G. Pushin, and A. N. Uksusnikov, "Influence of thermomechanical treatment on structural-phase transformations and mechanical properties of the Cu–Al–Ni shape-memory alloys," Russ. Phys. J. **61**, 1681–1686 (2018).
27. A. E. Svirid, A. V. Luk'yanov, V. V. Makarov, V. G. Pushin, and A. N. Uksusnikov, "Influence of doping with aluminum on the structure, phase transformations and properties of Cu–Al–Ni alloys with shape memory effect," Chelyabinskii Fiz.-Mat. Zh. **4**, 108–117 (2019).

Translated by T. Gapontseva